

# Model-based Crack Width Estimation using Rectangle Transform

Christian Benz  
Computer Vision in Engineering  
Bauhaus-Universität Weimar, Germany  
christian.benz@uni-weimar.de

Volker Rodehorst  
Computer Vision in Engineering  
Bauhaus-Universität Weimar, Germany  
volker.rodehorst@uni-weimar.de

## Abstract

The automated image-based robust estimation of crack widths in concrete structures forms a significant component in the automation of structural health monitoring. The proposed method, called rectangle transform, uses the gray-scale profile extracted perpendicularly to the direction of crack propagation. Based on the concept of an idealized profile, it transforms the empirical profile into an equal-area rectangle from which the width is inferred. On the available dataset and compared to two other approaches, it shows at least par performance for widths larger two pixels and distinctly better performance on widths smaller equal two pixels. Moreover, it is more robust towards blurred input.

## 1 Introduction

The process of digitization in the field of civil engineering is taking up pace [1, 2, 3]. With increasing robustness and quality of data acquisition platforms – such as e.g. drones – more and more domain relevant data becomes available. One potential usage of the growing amount of data is to advance the automation of traditionally resource-intensive processes.

In the area of structural health monitoring, advanced image acquisition platforms can be used to capture high quality imagery of the surface of critical infrastructure. These images can serve various purposes, such as the reconstruction of 3D models, maintaining a digital twin of the structure, or the (semi-)automated detection of defects. Among structural defects *cracks* form a class of special interest as their length, width, shape, and position offer significant insights into the structure’s health.

In this work the focus is on the automated measurement of the *width* of cracks based on their gray-scale profile. In order to obtain the gray-scale profile, the crack is assumed to have been tagged on the image – automatically or manually – and the profile perpendicular to the propagation direction of the crack to be extracted. The process of crack detection [4, 5, 6] and profile extraction is not part of this work.

The contribution of this work is threefold: (1) It provides an analysis of empirically occurring gray-scale profiles of cracks. (2) By the acquisition of specific data, it attempts to bridge the gap between crack widths

measured manually on-site and on image level. And (3) it provides a theoretically justified algorithm for subpixel-accurate estimation of the crack width.

## 2 Related Work

The automated estimation of crack widths from images is an active research field for at least the last decade. Many approaches rely on the accurate binarization of the image while others use gray-scale profiles or proper moments for width estimation.

Analogously to stroke width transform, [7] design a *crack width transform* (CWT) method. Starting from one edge, the algorithm determines the opposing edge and allocates the width in between. The CWT shows to be superior to line enhancement filtering as based on Frangi [8], which amplifies high-frequency structures. A similar edge-based procedure is applied in [9].

Different adaptive thresholding approaches for width estimation are evaluated in [10]. Different window sizes and sensitivity levels yield different binarized version of the image. By extraction of the binary profile perpendicular to the direction of crack propagation, the width can be directly inferred. The results are evaluated against widths measured by means of an optical microscope. Having three-dimensional data at hand [11, 12] determine a binary representation of the data by thresholding the local normal deviation from the context normal. [13] obtain a binary representation of

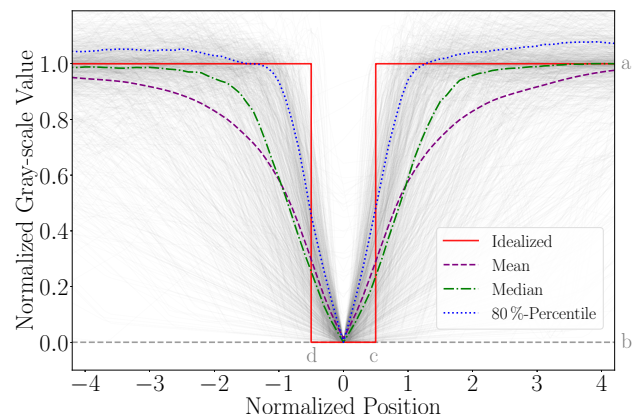


Figure 1: Normalized gray-scale profiles of cracks.

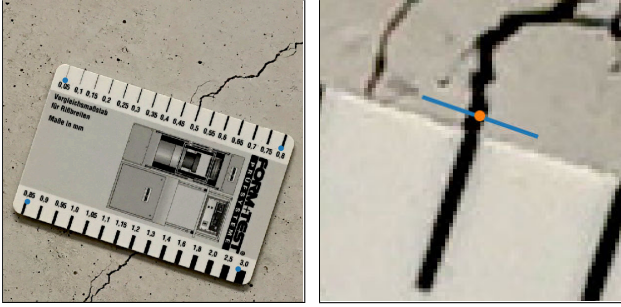


Figure 2: Left: Measurement gauge for crack width. Right: Extraction line for gray-scale profile perpendicular to the propagation direction of the crack.

the image by designing a convolutional neural network with crack-like shaped kernels for crack detection. The width is computed by Euclidean distance transform. For [14] a percolation-based approach to crack detection [15, 16] returns a binary crack map. Alongside this map and background correction, the crack width is determined through a procedure of iterative thinning.

The approach by [17] makes use of the Zernike polynomials [18]. Applying the zero-repetition second and fourth order Zernike moment operator, a given crack patch is rotation-invariantly transformed into complex-valued polynomials. By integration the polynomials yield a direct solution for crack width.

Based on the extraction of the gray-scale profile, [19] propose an approach that relies on iteratively fitting a parabola into the crack profile (*parabola fitting*). In the first step, all values from the profile are removed that lie within three standard deviations (i.e. 99.7%) of the difference between profile and fitted parabola. In the subsequent steps, values are removed that are outside of three standard deviations.

Most of the approaches are designed for properly sampled cracks, but struggle with crack widths smaller than a couple of pixels. Furthermore, many approaches have a noticeable number of hyperparameters that need to be tuned. Also, some approaches lack robustness with respect to the number of sampling points and blurry input.

### 3 Data

In order to bridge the gap between synthetic and real-world data, the acquisition of a dataset was conceptualized and conducted. It is based on the assumption, that synthetic data can by no means model the imperfections in the image capturing process induced by e.g. noise or effects related to camera lens or sensor.

#### 3.1 Acquisition

The general procedure for capturing a sample for the dataset was to manually measure a crack with the *measurement gauge*. This gauge – shown in Figure 2 (left) – is 85 mm wide and 53.5 mm high and offers width templates in steps of 0.05 mm for smaller widths (0.05 - 1.2 mm) and larger and variously spaced steps for widths from 1.3 - 3.0 mm. Aligning the measured crack, the gauge was attached to the structure and pictures were taken from different distances and slightly different (but still nearly orthogonal) perspectives. For image capturing, a Sony Alpha 7R I with lenses of 55 mm and 85 mm was placed on a tripod.

The images then were manually annotated by marking salient points on the gauge and the placement of the crack profile, cf. Figure 2. From the salient points the resolutional translation from mm to px and, thus, the expected crack width in px could be inferred.

As shown in Table 1 images were captured from four different structures, 979 images in total. From each crack measurement 8.5 images were taken on average. The acquisition distance ranges between roughly 1 to 3 m. The structures differ with respect to the number of cracks measured at a structure and the average widths of the cracks, which induces a bias towards crack widths under 2 px.

#### 3.2 Profile

In order to obtain an averaged representation of the gray-scale profile of cracks, all 979 profiles are extracted. For aligning all cracks, both x- and y-axis need to undergo normalization. Given that  $w_t$  is the true width,  $g(x)$  the gray-scale function that maps from position  $x$  to gray value  $g(x)$  and  $g_c(x) = x + \arg \min_x g(x)$  centers the profile around origin 0, then the following

Structure	#Images	#Measurements	Images per Measure.	Width [mm]			Width [px]			Avg. Distance [m]
				Mean	Median	Vari.	Mean	Median	Vari.	
BridgeB	54	12	4.5	0.531	0.450	0.024	5.263	4.562	8.356	1.37
BridgeS	748	76	9.8	0.122	0.100	0.003	1.300	0.901	1.260	1.86
BridgeU	41	8	5.1	0.135	0.150	0.002	1.642	1.394	1.048	1.11
Indoors	136	19	7.2	0.475	0.500	0.057	3.333	2.966	4.579	1.82
Total	979	115	8.5	0.194	0.150	0.033	1.815	1.137	3.283	1.79

Table 1: Overview of the available data and the respective crack widths.

normalization was performed:

$$g_{\text{norm}}(x) = \frac{g_c(x/w_t) - \min g(x)}{\text{median}(g_c(x)) - \min g(x)}$$

Figure 1 shows the average profiles alongside all profiles (light gray). Purple (dashed) represents the mean, green (dash-dotted) the median profile, and blue (dotted) the 80%-percentile. The profiles originate at the centralized minimum and rather steeply and symmetrically gain height until saturating at around 1. The mean reacting sensitively to low outliers in the peripheral area, while the median and 80%-percentile earlier reach the level of saturation. The red graph represents the *idealized profile* of a crack with infinitely steep flanks captured at virtually infinite sampling rate.

## 4 Rectangle Transform

The basis for the model-based approach is formed by the concept of an *idealized profile* of a crack as introduced in the last section and shown in Figure 1 (red). Based on the context gray value ( $a$ ), the bottom gray level ( $b$ ), the right flank position ( $c$ ), and the left flank position ( $d$ ), the *width* ( $w$ ) of the crack and the *height* ( $h$ ) of the profile can be computed by:

$$h = a - b \quad (1)$$

$$w = c - d \quad (2)$$

If  $c$  and  $d$  are known, the width  $w$  can be directly determined. For empirical cases, however,  $c$  and  $d$  are typically unknown. Based on the assumption that  $h$  and  $w$  form a *rectangle* with area  $A$  such that:

$$A = h \cdot w \quad (3)$$

$$w = \frac{A}{h} \quad \Leftrightarrow \quad w = \frac{A}{a - b} \quad (4)$$

an estimate for  $w$ , called  $\hat{w}$ , can be obtained through estimates for  $A$ ,  $a$ , and  $b$ :

$$\hat{w} = \frac{\hat{A}}{\hat{a} - \hat{b}} \quad (5)$$

Reasonable, empirically sound estimates for  $a$  and  $b$  are given by the reduced adapted median and the selective minimum:

$$\hat{a} = (\text{median}(g(x)) - \min(g(x))) \cdot 0.9 + \min(g(x)) \quad (6)$$

$$\hat{b} = \min(g(x), 20) \quad (7)$$

For the bottom gray level,  $\hat{b} = 0$  did not serve as a good estimate, presumably because the amount of light escaping the crack is larger zero. Empirically, 20 appeared a suitable value. For area  $\hat{A}$  holds (under omission of integration constants):

$$\hat{A} = \int (\hat{a} - \min(g(x), \hat{a})) \, dx \quad (8)$$

$$= \int \hat{a} \, dx - \int \min(g(x), \hat{a}) \, dx \quad (9)$$

$$= \hat{a}x - \int \frac{g(x) + \hat{a} - |g(x) - \hat{a}|}{2} \, dx \quad (10)$$

$$= \hat{a}x - \frac{1}{2} \int (g(x) + \hat{a} - |g(x) - \hat{a}|) \, dx \quad (11)$$

$$= \frac{1}{2} \left( \hat{a}x - \int (g(x) - |g(x) - \hat{a}|) \, dx \right) \quad (12)$$

Thus,  $\hat{w}$  can be determined from estimates for  $A$ ,  $a$ , and  $b$  without recourse to the unknowns  $c$  and  $d$ :

$$\hat{w} = \frac{\hat{a}x - \int (g(x) - |g(x) - \hat{a}|) \, dx}{2(\hat{a} - \hat{b})} \quad (13)$$

Width $w$ [px]	Approach	MAE		MAPE	Response Rate	Tolerance Interval [mm]			
		[px]	[mm]			$\leq 0.025$	$\leq 0.05$	$\leq 0.1$	$\leq 0.2$
$0 < w \leq 2$	Intersect	0.627	0.234	1.900	99.6 %	20 %	34 %	60 %	93 %
	Parabola	0.778	0.117	<b>0.760</b>	7.7 %	3 %	4 %	7 %	94 %
	Rectangle	<b>0.273</b>	<b>0.105</b>	0.782	<b>100.0 %</b>	<b>53 %</b>	<b>78 %</b>	<b>92 %</b>	<b>98 %</b>
$2 < w \leq 15$	Intersect	0.905	0.087	0.222	<b>100.0 %</b>	21 %	41 %	67 %	91 %
	Parabola	1.098	0.114	0.271	85.4 %	19 %	43 %	63 %	90 %
	Rectangle	<b>0.572</b>	<b>0.055</b>	<b>0.146</b>	<b>100.0 %</b>	<b>38 %</b>	<b>67 %</b>	<b>86 %</b>	<b>97 %</b>
$0 < w \leq 15$	Intersect	0.709	0.191	1.405	99.7 %	20 %	36 %	62 %	93 %
	Parabola	1.042	0.114	<b>0.357</b>	30.5 %	8 %	16 %	23 %	91 %
	Rectangle	<b>0.361</b>	<b>0.091</b>	0.595	<b>100.0 %</b>	<b>49 %</b>	<b>75 %</b>	<b>91 %</b>	<b>97 %</b>
$0 < w \leq 15$ , blur, $\sigma = 2$	Intersect	2.083	0.412	3.664	99.0 %	7 %	12 %	21 %	37 %
	Parabola	1.866	0.168	<b>0.377</b>	14.1 %	0 %	1 %	6 %	64 %
	Rectangle	<b>0.416</b>	<b>0.093</b>	0.568	<b>100.0 %</b>	<b>35 %</b>	<b>67 %</b>	<b>90 %</b>	<b>98 %</b>
$0 < w \leq 15$ , blur, $\sigma = 4$	Intersect	4.098	0.736	6.264	95.0 %	1 %	3 %	7 %	20 %
	Parabola	4.131	0.336	<b>0.421</b>	0.9 %	0 %	0 %	0 %	33 %
	Rectangle	<b>0.798</b>	<b>0.119</b>	0.678	<b>100.0 %</b>	<b>14 %</b>	<b>33 %</b>	<b>70 %</b>	<b>91 %</b>

Table 2: Overview of the results for different approaches and crack widths.

Conceptually, the approach transforms the area inside the “sink” of the crack profile into an equal-area rectangle. This rectangle is presumed to resemble the alleged original signal. **Rectangle transform**, thus, appears to be a descriptive name for the approach.

## 5 Evaluation

Table 2 provides an overview of the results. It shows the performance of the three approaches *naïve intersection* (“Intersect”), *parabola fitting* (“Parabola”), and *rectangle transformation* (“Rectangle”) with respect to different crack widths and levels of Gaussian blur. In parabola fitting [19], gray values undergo a statistically-guided, iterative removal and a parabola is fit on the remaining values. The width is estimated based on the intersection of the fitted parabola and the 50% mean intensity value. The naïve intersection approach also relies on intersection for width estimation. It, however, intersects the intensity profile itself, rather than a fitted function, with the 30% adapted median of the profile.

MAE refers to the *mean average error*, MAPE to the *mean average percentage error* which relates the error to the ground truth value. Since many values are located in the range of -1 and 1, the MAE occurs a more reasonable measure than the *mean squared error*. The *response rate* describes the share of data for which an estimate was returned. The *tolerance interval* denotes the proportion of responses within the given interval. Note that the interval  $\leq 0.025$  can be considered to reflect the unavoidable measurement inaccuracy induced by the stepping properties of the measurement gauge.

With respect to widths less or equal 2 px, the rectangle approach provides the only robust estimate. It shows the lowest MAE and has a perfect response rate. The MAPE is comparable to the parabola approach, which, however, has a noticeably low response rate of 8%. Also with respect to the tolerance interval, rectangle surpasses the other approaches with 98% for the 0.2 mm interval. For widths larger than 2 px, all approaches have lower MAPE, i.e. perform better in relative terms. As far as response rates are concerned, only the intersection and rectangle approach achieve 100% while the parabola secedes. One reason for the better average performance for wider cracks is potentially rooted in the sampling theorem, according to which only cracks wider 2 px are properly sampled [20]. The aggregated results for widths 0 to 15 px confirm the superiority of rectangle transform for the given dataset.

Even though undesired, lack of image sharpness regularly occurs in images and genuinely impedes the width estimation. To simulate lack of sharpness, Gaussian blur was applied on the gray-scale profile. When confronted with blurred input (Table 2, bottom) all approaches degrade in performance. The only approach producing relatively consistent estimates is rectangle transform while intersection and parabola approach deteriorate.

Figure 3 depicts the relation of widths between 0 px

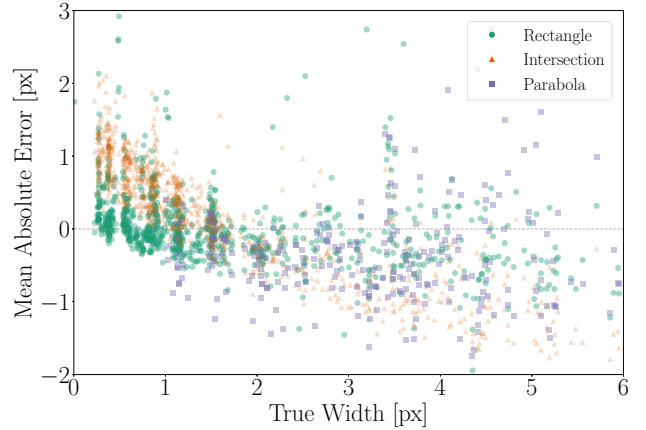


Figure 3: Overview of the performance.

and 6 px and the MAE. The clustered predictions for widths less 2 px exemplify the bias in the data towards smaller widths. For this range the estimates from the rectangle approach cluster around zero MAE, while the intersection approach shows a tendency for overestimation. The parabola approach only sparsely returns estimates for width smaller than 2 px which corresponds to its low response rate for this range. For widths larger 2 px the variance increases for all approaches with a general tendency to slight underestimation.

## 6 Conclusion

The experimental results demonstrate the higher robustness of the rectangle transform compared to naïve intersection and parabola fitting. This robustness refers to the quality of measurements for blurred inputs as well as the generally perfect response rate. However, these results are obtained in a relatively restrictive setup with one type of camera. It is unclear in how far the parameters require adaptation in order to achieve equal performance in a different setup. The theoretical derivation, hopefully, provides a solid basis for generalization.

For all approaches holds, the wider the cracks in pixels and the lower the blur, the better the estimate. Thus, for practical purposes it is advisable to capture cracks as close and as well resolved as possible, rather than pushing acquisition to the photographic limits.

Despite the many advantages that theory-driven approaches have, data-driven ones hold the potential for better estimates given that a large and representative dataset is available. The acquisition procedure proposed here comes with a multitude of flaws. It, however, is (to the best of our knowledge) the first honest, wide-range attempt to bridge the gap between image level and manual onsite measurement. With more data at hand, convolutional learning approaches that directly operate on image level rather than gray-scale profiles become in graspable range.

## References

- [1] D. Kang and Y.-J. Cha, "Autonomous UAVs for structural health monitoring using deep learning and an ultrasonic beacon system with geo-tagging," *Computer-Aided Civil and Infrastructure Engineering*, vol. 33, no. 10, pp. 885–902, 2018.
- [2] T. Khuc and F. N. Catbas, "Completely contactless structural health monitoring of real-life structures using cameras and computer vision," *Structural Control and Health Monitoring*, vol. 24, no. 1, p. e1852, 2017.
- [3] S. Sony, S. Laventure, and A. Sadhu, "A literature review of next-generation smart sensing technology in structural health monitoring," *Structural Control and Health Monitoring*, vol. 26, no. 3, p. 2321, 2019.
- [4] Y. Liu, J. Yao, X. Lu, R. Xie, and L. Li, "Deepcrack: A deep hierarchical feature learning architecture for crack segmentation," *Neurocomputing*, vol. 338, pp. 139–153, 2019.
- [5] A. Mohan and S. Poobal, "Crack detection using image processing: A critical review and analysis," *Alexandria Engineering Journal*, vol. 57, no. 2, pp. 787–798, 2018.
- [6] Q. Zou, Z. Zhang, Q. Li, X. Qi, Q. Wang, and S. Wang, "Deepcrack: Learning hierarchical convolutional features for crack detection," *IEEE Transactions on Image Processing*, vol. 28, no. 3, pp. 1498–1512, 2018.
- [7] H. Cho, H.-J. Yoon, and J.-Y. Jung, "Image-based crack detection using crack width transform (cwt) algorithm," *IEEE Access*, vol. 6, pp. 60100–60114, 2018.
- [8] A. F. Frangi, W. J. Niessen, K. L. Vincken, and M. A. Viergever, "Multiscale vessel enhancement filtering," in *International Conference on Medical Image Computing and Computer-assisted Intervention*, pp. 130–137, Springer, 1998.
- [9] Y.-F. Liu, X. Nie, J.-S. Fan, and X.-G. Liu, "Image-based crack assessment of bridge piers using unmanned aerial vehicles and three-dimensional scene reconstruction," *Computer-Aided Civil and Infrastructure Engineering*, vol. 35, no. 5, pp. 511–529, 2020.
- [10] H. Kim, E. Ahn, S. Cho, M. Shin, and S.-H. Sim, "Comparative analysis of image binarization methods for crack identification in concrete structures," *Cement and Concrete Research*, vol. 99, pp. 53–61, 2017.
- [11] J. Valença, D. Dias-da Costa, E. Júlio, H. Araújo, and H. Costa, "Automatic crack monitoring using photogrammetry and image processing," *Measurement*, vol. 46, no. 1, pp. 433–441, 2013.
- [12] J. Valença, I. Puente, E. Júlio, H. González-Jorge, and P. Arias-Sánchez, "Assessment of cracks on concrete bridges using image processing supported by laser scanning survey," *Construction and Building Materials*, vol. 146, pp. 668–678, 2017.
- [13] J. S. Lee, S. H. Hwang, I. Y. Choi, and Y. Choi, "Estimation of crack width based on shape-sensitive kernels and semantic segmentation," *Structural Control and Health Monitoring*, vol. 27, no. 4, p. e2504, 2020.
- [14] T. Yamaguchi and S. Hashimoto, "Practical image measurement of crack width for real concrete structure," *Electronics and Communications in Japan*, vol. 92, no. 10, pp. 1–12, 2009.
- [15] T. Yamaguchi and S. Hashimoto, "Image processing based on percolation model," *IEICE Transactions on Information and Systems*, vol. 89, no. 7, pp. 2044–2052, 2006.
- [16] T. Yamaguchi and S. Hashimoto, "Fast crack detection method for large-size concrete surface images using percolation-based image processing," *Machine Vision and Applications*, vol. 21, no. 5, pp. 797–809, 2010.
- [17] F. Ni, J. Zhang, and Z. Chen, "Zernike-moment measurement of thin-crack width in images enabled by dual-scale deep learning," *Computer-Aided Civil and Infrastructure Engineering*, vol. 34, no. 5, pp. 367–384, 2019.
- [18] F. Zernike, "Beugungstheorie des Schneidenverfahrens und seiner verbesserten Form, der Phasenkontrastmethode," *Physica*, vol. 1, no. 7-12, pp. 689–704, 1934.
- [19] V. Haaf, "Bildanalyse zur Erkennung und Vermessung von Betonrissen," Bachelor thesis, 2015.
- [20] C. E. Shannon, "Communication in the presence of noise," *Proceedings of the IRE*, vol. 37, no. 1, pp. 10–21, 1949.